Real-Time Shape Evolution of Nanoimprinted Polymer Structures during Thermal Annealing

Ronald L. Jones,[*,†,§] **Tengjiao Hu,**[†] **Christopher L. Soles,**[†] **Eric K. Lin,**[†]
Ronald M. Reano,[‡] **Stella W. Pang,**[‡] **and Diego M. Casa**[||]

*Polymers Division, National Institute of Standards and Technology, Gaithersburg,
Maryland 20899, Department of Electrical Engineering and Computer Science,
University of Michigan, Ann Arbor, Michigan 48109, and CMC-CAT, Advanced
Photon Source, Argonne National Laboratory, Argonne, Illinois 60439*

ABSTRACT

The real-time shape evolution of nanoimprinted polymer patterns is measured as a function of annealing time and temperature using critical dimension small-angle X-ray scattering (CD-SAXS). Periodicity, line width, line height, and sidewall angle are reported with nanometer resolution for parallel line/space patterns in poly(methyl methacrylate) (PMMA) both below and above the bulk glass transition temperature (T_G). Heating these patterns below T_G does not produce significant thermal expansion, at least to within the resolution of the measurement. However, above T_G the fast rate of loss in pattern size at early times transitions to a reduced rate in longer time regimes. The time-dependent rate of polymer flow from the pattern into the underlying layer, termed pattern "melting", is consistent with a model of elastic recovery from stresses induced by the molding process.

Nanoimprint lithography (NIL) is a low-cost, effective nanofabrication tool for patterning arbitrary structures with critical dimensions (CD) well below 100 nm.[1,2] To date, novel patterns with feature sizes less than 5 nm have been demonstrated.[3,4] The maturation of NIL as a pattering technology is reflected by its inclusion as a potential next-generation lithography in the International Technology Roadmap for Semiconductors.[5] Looking beyond semiconductors, the potential of NIL to pattern polymers of arbitrary chemistry and/or architecture promises to provide functional patterns (e.g., patterns that perform an electrical, optical, mechanical, structural, biomedical, etc. task) that can be built *directly* into nanometer-scale devices. This is generally not possible with state-of-the-art optical lithographies where the polymeric patterns are used as a sacrificial resist. However, the end use of a polymer nanostructure as a device, such as in micro- or nanofluidic channels, organic semiconductors, sensors, photonic devices, and so forth, requires a broad understanding of pattern stability outside of the mold (i.e., "free-standing"), both over time and with varying environmental conditions. Pattern stability, for example, is expected

to result from a balance of viscosity, internal stresses from the molding process, and surface tension. For feature sizes ≪100 nm, stability is anticipated to be a significant issue in light of the reductions in viscosity or glass transition observed both at polymer surfaces and in ultrathin films.[6−9] Understanding the relative roles of pattern size, shape, environmental conditions, and bulk material properties requires precise measurements of shape in polymeric NIL patterns as a function of processing parameters.

Here we present data on pattern stability (after removal of the mold) as a function of annealing temperature, both below and above the bulk glass transition temperature (T_G), for parallel line/space patterns imprinted into PMMA. Stability is quantified by measuring the rate of change in the average cross-sectional shape of the lines. Real-time pattern shape is obtained using critical dimension small-angle X-ray scattering (CD-SAXS).[10,11] CD-SAXS is capable of measuring the cross section of periodic patterns ranging from 10 to 500 nm in width; the width of the patterns here was ∼100 nm. The CD-SAXS measurements are nondestructive, with subnanometer precision, and capable of quantifying lines directly supported on a hard Si substrate. We note that electron microscopy techniques, which are also capable of similar studies, are often destructive to polymer films and make a study of stability, especially at high temperatures, challenging. This study is conceptually similar to those of

---

  * Corresponding author. E-mail: ronald.jones@nist.gov.
  † National Institute of Standards and Technology.
 ‡ University of Michigan.
  § Official contribution of the National Institute of Standards and Technology; not subject to copyright in the United States.
  || Argonne National Laboratory.

Johannsmann and co-workers where large-scale sinusoidal patterns with ~1 μm periodicity were pressed into a bulk polymer surface.[12,13] Reflected laser light scattering off of the patterned surface was used to track the decay of the pattern height at elevated (above T_G) temperature. A simple sinusoidal pattern was chosen to study surface rheological properties to avoid complications due to pattern shape. In this work, the two-dimensional pattern cross section is tracked explicitly as the long-range ordered pattern flows into the underlying polymer film. Because this process reduces the amount of volume of long-range ordered patterned material, we label this process as pattern "melting"; however, we stress that the polymer itself is not crystalline and the melting only refers to the overall long-range order of the pattern itself.

NIL and CD-SAXS. Films of atactic poly(methyl methacrylate) (PMMA) were spun-cast from toluene on SEMI-standard 200-mm-diameter silicon wafers with an unpatterned thickness of ~500 nm. PMMA was purchased from Microchem Inc.[14] with a molecular mass of 15 000 $M_{r,n}$ and polydispersity of 2.2. The calorimetric glass transition temperature (T_G) of this PMMA was 86 ± 1 °C, as determined from the midpoint of the inflection on a heat capacity curve.[15] The nanoimprint mold consisted of a set of parallel lines and spacings with a line/space ratio of approximately 1:1. The mold was fabricated in silicon oxide via 193 nm optical photolithography using a JSR 1237R resist on a 200 mm SEMI-standard Si wafer. Nanoimprint lithography was performed on an Obducat NIL 4 (Series 1) machine. Imprinting was conducted in the thermal embossing mode for 10 min at a temperature of 190 °C and a pressure of 6 MPa. Subsequently, the mold was cooled to below T_G before the sample was removed from the mold. Cross-sectional SEM images reveal a residual, unpatterned layer that is ~200 nm thick.

Details of the CD-SAXS technique are described elsewhere.[10,11] Briefly, the technique uses transmission small-angle X-ray scattering though the supporting Si wafer, treating the polymer pattern as a diffraction grating. The diffraction peak spacing is given by $\Delta q = 2\pi/L$, where L is the pattern period, $q = 4\pi/\lambda \sin(\theta)$, λ is the X-ray wavelength, and 2θ is the scattering angle as measured along the axis of diffraction (see Figure 1). Parameters describing the pattern cross section are determined by the relative intensity of the peaks at varying angles of incidence, ω, with $\omega = 0°$ defined as the incident beam normal to Si wafer. The CD-SAXS measurements were performed at the 9ID-CMC beamline of the Advanced Photon Source (Argonne National Laboratory) using a two-dimensional CCD detector. The X-ray wavelength was set to 1.1106 ± 0.0001 Å using a double monochromator and collimating optics that include dual focusing mirrors and two sets of slits. This produces a final beam of size 80 × 80 μm² at the sample position. A 1024 × 1024 pixel CCD X-ray detector was placed 583 ± 1 cm from the sample. To compare scattering data at different rotation angles, ω, corrections were made for the angle-dependent attenuation factor, beam path length, and beam spot size on the sample.
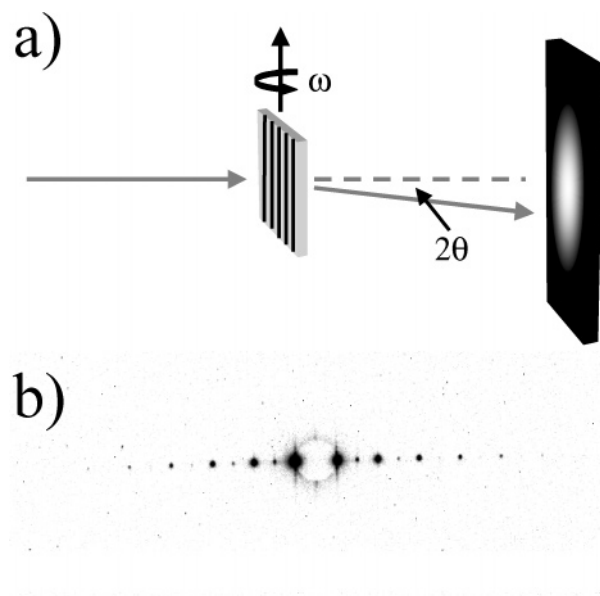

Figure 1. Schematic of the CD-SAXS geometry (a), showing the incident X-ray beam, the sample rotated at an angle ω, and the diffracted beam at the scattering angle 2θ as measured on a 2D detector. In part b is the resulting 2D diffraction pattern recorded for a nanoimprinted PMMA sample, showing the characteristic 1D diffraction pattern.

The patterned samples were mounted on an aluminum heating stage with a small slit machined into the center of the stage to allow transmission of the X-ray beam. The Si wafer supporting the patterns was mounted onto the stage with thermal paste, and the temperature was calibrated using a similarly mounted blank SEMI-standard wafer with a thermocouple attached to the free surface, providing a master curve to correlate the temperature at the silicon surface with the controller readout temperature. This master curve was calibrated by recording the melting points of three well-known solids (orthoterphenol, 58.0 °C; benzoic acid, 121.5 °C; indium, 156.6 °C) supported on the blank Si wafer.

Dimensions at Sub-T_G Temperatures. For temperatures $T < T_G$ of the PMMA, CD-SAXS data were collected for ω ranging from ca. −20° to +20° with a step size of 1 ± 0.0005°. Samples were equilibrated at each T for 60 min, with a subsequent 80 min required to collect data over the full ω range. Using a rotation matrix, the data from different ω are converted to an effective q_x−q_z plane, where q_x and q_z are reciprocal space vector components of q that are parallel and perpendicular to the Si substrate, respectively. The data are then compared to the two-dimensional Fourier transform of a model line cross section in the q_x−q_z plane. As detailed elsewhere,[11] the average cross section is modeled as a trapezoid, where the fitting parameters are the average line width W, line height H, and sidewall angle β ($\beta = 0$ represents a vertical sidewall).

The nanoimprinted PMMA line/space patterns were evaluated at several temperatures below the bulk T_G. Figure 2a illustrates representative CD-SAXS data from a sample at 42 °C over the full range of rotation angles. At T far below T_G, the patterns were stable and the scattering intensities were time-independent over the 80 min required to collect a full
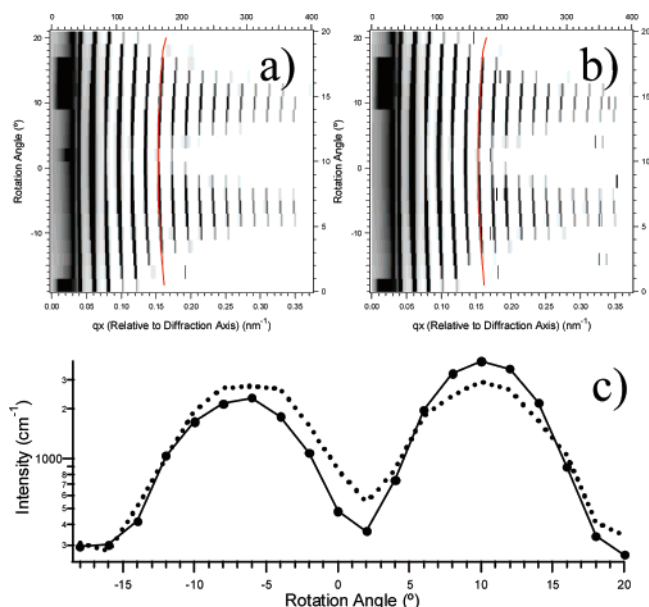
Figure 2. Experimentally measured CD-SAXS data as a function of rotation angle below T_G (a) compared to the analogous results from a trapezoidal model as described in the text (b). Intensities from a single Bragg diffraction peak contour are provided as a function of rotation angle, ω, in part c, comparing experimental results (solid circles) to model data (solid line).

rotation data set. This suggests that the PMMA is not degraded or damaged by the X-ray beam. The scattering pattern in Figure 2a is characteristic of a trapezoidal cross section,[11] with horizontal ridges of intensity emanating at $\omega = \pm\beta$. The presence of these ridges can establish the validity of a particular scattering model prior to the full implementation of the fitting procedure. At $T = 42$ °C, the best-fit trapezoidal model, shown in Figure 2b, yields a periodicity $L = 325 \pm 1$ nm, an average line width $W = 134 \pm 1$ nm, a sidewall angle $\beta = 7.0 \pm 0.5°$, and a line height $H = 320 \pm 10$ nm. Notice that the precision of L ($\Delta L/L = 0.004$) and W ($\Delta W/W = 0.007$) are significantly better than H ($\Delta H/H = 0.03$). Although each of these parameters contributes to the entire scattering $q_x - q_z$ plane, the primary contribution of pattern height is the periodic fringes in the scattered intensity that propagate along the curved vertical contours in Figure 2a and b. The intensity distribution along one of these contours is shown in Figure 2c. These fringes are of lower intensity because of the lack of periodicity in the sample perpendicular to the substrate, with only two or three orders of intensity appearing above the background of the instrument. Enhanced precision in H may result from reducing the background noise through, for instance, the use of low-noise detectors. Further increases in precision are also possible by expanding the range of ω, effectively increasing the q_z range measured. Finally, using a smaller step size in ω would increase the number of data points per fringe and decrease the uncertainty.

The pattern dimensions listed above were measured over a T range from room temperature to 60 °C (all sub-T_G). However, changes in the pattern dimension with T were not observed to within experimental error; thermal expansion or contraction below T_G was not apparent. This result is not

unexpected given the uncertainty of $\Delta W = \pm 1$ nm. The bulk linear thermal expansion coefficient for glassy PMMA is on the order of 5×10^{-5}/°C. A $\Delta T = 149$ °C is required to induce $\Delta W = 1$ nm in a 134-nm-thick PMMA line; observing subnanometer thermal expansion is currently beyond the resolution limit of this measurement method. To achieve this level of precision, the sample must produce a larger number (>30) of diffraction peaks to increase the precision of W significantly. Random variations in line width within the beam spot also lead to a monotonic decay of peak intensity at higher q, mathematically described by a Debye−Waller factor. Subnanometer precision thermal expansion measurements would be significantly easier if the sample quality was such that $|\Delta W/W| < 1$ nm over the beam spot size, thereby reducing the Debye−Waller factor. The Debye−Waller factor also has the potential to provide the magnitude of line edge roughness (LER); however, the precision possible for LER measurements are dependent on the accuracy and completeness of the model describing the average cross section.[11] This relationship makes LER determinations nontrivial.

Upon heating to $T = 96$ °C ($T_G + 10$ °C), the CD-SAXS profile changed within the 80 min measurement time, indicating changes in the shape of the patterns. Additional measurements at $T = 105$ °C showed a complete loss of diffraction after 1 h of annealing. Significant changes in dynamics of pattern evolution occur in the range of 96 to 105 °C.

Dynamics of Pattern Shape Evolution at Temperatures Greater than T_G. To further probe the kinetics of the shape evolution of these structures, a second sample imprinted under identical conditions was mounted at room temperature and ramped to 101 °C at a rate of 20 °C/min. CD-SAXS data collection commenced when the sample reached 101 °C. In contrast to the sub-T_G measurements, data were collected only at normal incidence rather than the full range of ω rotation. This reduces the measurement time to approximately 2 min per data set, but only provides length scales parallel to the substrate. High-precision measurements are limited to periodicity as well as top, bottom, and average line widths of the pattern. It is possible to infer the pattern height from changes in the total scattered intensity because the scattering intensity is proportional to the volume of material in the line. As the patterns "melt" into a smooth film, the scattering intensity decreases to zero. If the initial trapezoid cross section and the change in the pattern width with annealing time are known, then the decrease in the scattering intensity can be correlated to a decrease in pattern height assuming that the trapezoid model remains appropriate throughout the process. From these assumptions, the pattern height and sidewall angle are calculated from the $\omega = 0°$ CD-SAXS data as a function of annealing time at 101 °C.

Figure 3 shows a comparison of early ($t = 2$ min) and late ($t = 46$ min) stage scattering profiles of the nanostructures at $\omega = 0$ (i.e., no rotation). A reduction in overall diffracted intensity by a factor of 2 suggests a proportional loss of material from the periodic nanostructures into the underlying residual layer. We note that the residual layer
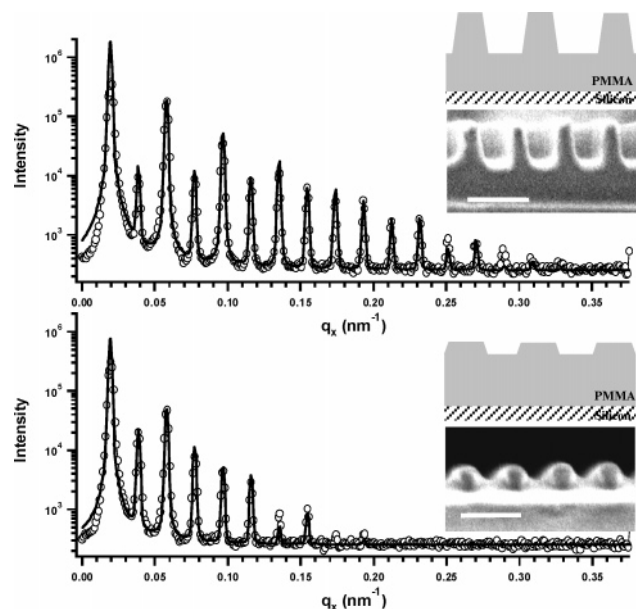
Figure 3. CD-SAXS diffraction spectrum taken at normal incidence to the sample after annealing for 2 min (top) and 46 min (bottom). Shown are the experimentally measured data (open circles) and the resulting model fits to a trapezoidal cross section (solid lines). The insets into each plot are scaled schematics of the resulting trapezoids and cross-sectional SEM's of representative samples described in the text. The scale bars in the SEM images indicate a length of 300 nm.

does not contribute to the diffraction peak intensity; a smooth film has no periodicity/structure within the plane of the film and does not diffract X-rays. From these data alone, it would be impossible to determine if the loss of intensity is due to material flow into the underlying residual layer, beam damage, or thermal decomposition. However, beam damage can be ruled out based on the sub-T_G measurements where the patterns were exposed to the X-ray beam for several hours without any change in the scattering intensity. Thermal decomposition is highly unlikely given that the annealing temperature is well below the degradation temperature of PMMA ($T_{\text{degradation}} > 200\ ^\circ$C). The only remaining possibility is that the intensity loss is primarily due to the flow of polymer into the underlying residual layer. Also evident in Figure 3 is the q dependence of the decay in the Bragg peak intensities; the decay is more significant at higher q. This behavior is characteristic of a growing distribution of periodicities and increasing sidewall angle. The relative intensity of the lowest order peaks is strongly dependent on the average line width, whereas the higher order peaks increasingly depend on the difference in the top and bottom widths.

The cross-sectional SEM images in Figure 3 further confirm that the trapezoidal line shape remains a reasonable approximation of the line cross section after 46 min of annealing. Figure 3a demonstrates a classic trapezoidal shape on a sample imprinted under the same conditions, and therefore approximates the $t = 0$ s state of the current experiment. The SEM image in Figure 3b is a cross-sectional image of the sample described here after 46 min of annealing and subsequent cooling. Although it is possible that the shape

changed further during cooling, the image demonstrates that a trapezoidal model is applicable and serves as a check on the dimensions from the CD-SAXS data at $t = 46$ min. Given the applicability of a trapezoidal model, the average line cross section evolves from a tall, vertical ($H = 210 \pm 10$ nm, $W = 141 \pm 1$ nm, $\beta = 5 \pm 1^\circ$) to a shorter, shallow ($H = 55 \pm 10$ nm, $W = 180 \pm 1$ nm, $\beta = 25 \pm 1^\circ$) trapezoid over the 46 min annealing period.

Figure 4 presents various aspects of the trapezoidal cross-section model parameters as a function of annealing time for the PMMA imprints at 101 °C. Data from the sub-T_G sample are included as the $t = 0$ s data points. Part A of Figure 4 shows the pattern height, H, decreasing continuously over the span of the experiment. An arbitrary exponential fit nominally parametrizes the t dependence. In Figure 4D, the derivative or slope of this fit shows that decay is more rapid in the early stage of annealing, decreasing initially from ~ 3 nm/s to ~ 0.01 nm/s at long times (2500 s). Likewise, Figure 4B shows the broadening of the pattern width (average, top, and bottom width of the trapezoid) over the same time interval. Exponential fits to these data and their derivatives are compared to the height in Figure 4D. Initially, the broadening rate of the line widths, ~ 1 nm/s, is of the same order of magnitude as the decay in the pattern height. However, by $t = 1000$ s the line width evolution slows down significantly to ~ 0.01 nm/s and remains nearly constant at longer times. Although the decay rate in pattern height also reaches a constant on the order of 0.01 nm/s, it does not approach this value until 2500 s; at 1000 s the rate of change in pattern height is still about 1 order of magnitude greater than the rate of change in pattern width.

Knowledge of the pattern height, top width, bottom width, and average width of the trapezoid allows us to calculate the time evolution of the sidewall angle, as shown in Figure 4C. The sidewall angle, β, in Figure 4 is inferred from the pattern widths and height and the assumption of a trapezoidal cross section, whereas the β from the sub-T_G data, where ω is rotated, is measured directly. It is interesting that the decay in β in Figure 4C more closely resembles the decay in H in part A than the increase in pattern width in part B; β and H appear to decay over similar time scales. This reflects the fact that the patterns shrink in height more rapidly than they broaden in width. It is important to realize that in the absence of broadening a reduction in height of a trapezoid naturally leads to an increase of β. For example, assume that the initial line widths of the trapezoid remained constant. A reduction of H from 210 to 55 nm with an initial $\beta = 5^\circ$ would then lead to a final $\beta = 18^\circ$. Given that the actual final $\beta = 25$ °C, the reduction of height dominates the change in β relative to the increase in W. This is also evident when considering that all three W values (top, bottom, and average) increase with t. If volume in the pattern was conserved, then the broadening of the bottom line width would be accompanied by a narrowing of the top width. However, volume is not conserved and material from within the pattern relaxes down into underlying film with annealing.

The fact that volume of material within the pattern is not conserved is verified from the scattering intensities. The
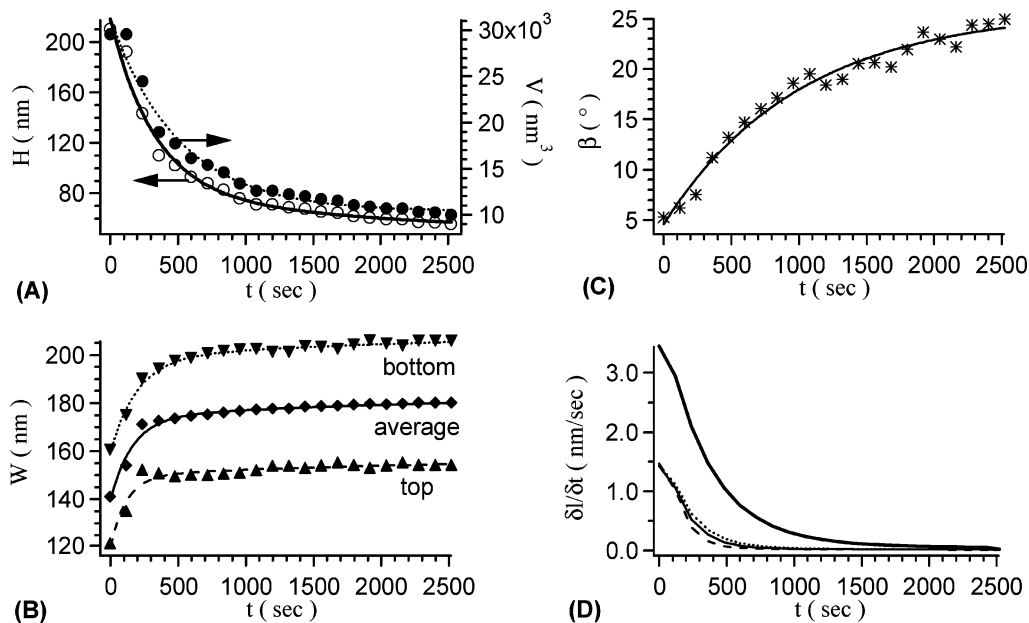
Figure 4. Parameters describing cross-sectional shape as a function of annealing time, t, at 101 °C. Shown in part A are the sample volume contributing to diffraction (grey circles) and the average pattern height (solid circles) with exponential fits to the height and volume as the solid and dashed lines, respectively. In part B, the top width (solid triangles), average line width (open circles), and bottom width (open triangles) are provided. The calculated sidewall angle (crosses) is given in part C with a fit to an exponential form (solid line). Derivative values, based on the exponential fits, of the height (thick solid line), top width (dashed line), average width (thin solid line), and bottom width (dot−dashed line) are plotted in part D. Also in part D is a linear fit used to obtain the rate dH/dt as described in the text (solid line).

decrease in the scattering intensity upon annealing, as evidenced in Figure 3, can be converted into a volume of material within the scattering pattern. The t dependence of this volume is also shown in Figure 4A. The decrease in pattern height tracks the decrease in scattering volume, indicating that the changes in H dominate the changes in the pattern shape. Remarkably, the polymer pattern decreases in height, but does not spread laterally even though the polymer does flow over laboratory time scales at these temperatures.

The nature of the change in the initial pattern shape, where the height of the pattern decays an order of magnitude faster than the increase in pattern width, is consistent with elastic recovery of the pattern from residual stresses inherent in the nanoscale molding process. This is in contrast to the work of Johannsmann[12,13] and co-workers who studied similar effects in PMMA surfaces perturbed with much larger wavelengths and significantly lower amplitude sinusoidal patterns. Assuming that the polymer acts as a Newtonian fluid with a constant surface tension, σ, they derived an expression for the change in the pattern height as a function of viscosity η and t: $dH/dt = (-\pi\sigma H)/(2L\eta)$ where L is the wavelength of the sinusoidal pattern. In their experiments, the decay in pattern height was linear with t because the wavelength of the sinusoidal pattern did not change with time. This linearity is not observed in Figure 4, presumably due to larger elastic stresses involved in molding much higher aspect ratio patterns. The data in Figure 4 show the line patterns withdrawing into, rather than spreading on, the underlying residual layer. As a result, it is natural to expect the residual layer to play an important role in the rate of decay. In the limit of large residual layers, the layer acts as

an infinite reservoir for the receding patterns. However, we may expect a critical residual layer thickness where the underlying substrate exerts control over the kinetics of decay. In this way, the interactions of the substrate and polymer layer may be an important factor in pattern stability.

At long times, however, the decay of pattern H can be approximated as linear. In this regime, we can compare the data to the model of Johannsmann to estimate of the polymer viscosity even though the patterns are not sinusoidal and L is comparable to the total film thickness. With $\sigma \approx 70$ mN/m for PMMA, we find $\eta \approx 1 \times 10^9$ Pa s when dH/dt approaches a constant value near $t = 2500$ s. Similar estimates at earlier times, for example at $t = 1000$ s and $t = 100$ s, where dH/dt increases significantly, consequently predict increasingly smaller viscosity of $\eta \approx 1 \times 10^8$ Pa s and $\eta \approx 1 \times 10^7$ Pa s, respectively. We can compare these values to the viscosity of bulk PMMA using the Williams−Landel−Ferry relationship $\eta/\eta_0 = C_1(T - T_0)/(C_2 + (T - T_0))$ where $\eta_0 (= 1 \times 10^{12}$ Pa s) and $T_0 (= 86$ °C) are a reference viscosity and temperature, and the constants C_1 $(= 70.1)$ and C_2 $(= -12.21)$ are empirically determined.[16] The viscosity predicted for bulk PMMA would be $\eta_{Bulk} = 7.9 \times 10^9$ Pa s. This indicates that late-stage evolution of the pattern approaches a regime that is dominated by simple bulk viscous flow, while the initial regimes are accelerated. It is also interesting that pattern broadening is more commensurate with the bulk viscous flow than the height reductions. Using more complete models should therefore provide a method to measure viscosity and surface stresses directly using CD-SAXS.

In conclusion, the cross-sectional shape and dimensions were quantitatively determined in real time for a polymer

grating produced by nanoimprint lithography. The CD-SAXS technique provided real-time measurements of shape during the melting of ordered nanoimprinted patterns at temperatures above the bulk T_G. For short times, a rapid decay from the original line shape with sharp corners at the edges is observed as the pattern evolves into a broadened trapezoid. The reductions in pattern height are much faster than the increasing of the pattern width, but both rates gradually approach values characteristic of the relaxation of small amplitude surface waves. Estimates of viscosity from the long time rates of pattern evolution are consistent with bulk values. Although the CD-SAXS technique currently provides significant detail on pattern shape and size, significantly more detail on polymer viscoelasticity is expected from more sophisticated models of the data.

References

(1) Heidari, B.; Maximov, I.; Sarwe, E.-L.; Montelius, L. *J. Vac. Sci. Technol., B* **1999**, *17*, 2961.

(2) Pang, S. W.; Tamamura, T.; Nakao, M.; Ozawa, A.; Masuda, H. *J. Vac. Sci. Technol.* **1998**, *16*, 1145.

(3) Austin, M. D.; Ge, H.; Wu, W.; Li, M.; Yu, Z.; Wasserman, D.; Lyon, S. A.; Chou, S. Y. *Appl. Phys. Lett.* **2004**, *84*, 5299.

(4) Hua, F.; Sun, Y.; Gaur, A.; Meitl, M. A.; Bilhaut, L.; Rotkina, L.; Wang, J.; Geil, P.; Shim, M.; Rogers, J. A.; Shim, A. *Nano Lett.* **2004**, *4*, 2467.

(5) 2004 International Technology Roadmap for Semiconductors: http://public.itrs.net.

(6) Kerle, T.; Lin, Z.; Kim, H.-C.; Russell, T. P. *Macromolecules* **2001**, *34*, 3484.

(7) Herminghaus, S.; Seemann, R.; Landfester, K. *Phys. Rev. Lett.* **2004**, *93*, 017801.

(8) Damman, P.; Baudelet, N.; Reiter, G. *Phys. Rev. Lett.* **2003**, *91*, 216101.

(9) Jones, R. A. L. *Curr. Opin. Colloid Interface Sci.* **1999**, *4*, 153.

(10) Jones, R. L.; Hu, T. J.; Lin, E. K.; Wu, W.-L.; Kolb, R. K.; Casa, D. M.; Boulton, P.; Barclay, G. G. *Appl. Phys. Lett.* **2003**, *83*, 4059.

(11) Hu, T. J.; Jones, R. L.; Lin, E. K.; Wu, W.-L.; Keane, D.; Weigand, S.; Quintana, J. P. *J. Appl. Phys.* **2004**, *96*, 1983.

(12) Hamdorf, M.; Johannsmann, D. *J. Chem. Phys.* **2000**, *112*, 4262.

(13) Petersen, K.; Johannsmann, D. *J. Non-Cryst. Solids* **2002**, *307*, 532.

(14) Certain commercial equipment and materials are identified in this paper in order to specify the experimental procedure adequately. In no case does such specification imply recommendation by the National Institutes of Standards and Technology nor does it imply that the material or equipment specified is necessarily the best available for this purpose.

(15) The data in this manuscript and in the figures are presented along with the standard uncertainty ($\pm$) involved in the measurement, where the uncertainty represents one standard deviation from the mean.

(16) Hartschuh, R.; Ding, Y.; Roh, J. H.; Kisliuk, A.; Sokolov, A. P.; Soles, C. L.; Wu, W.-L.; and Mahorowala, A. P. *J. Polym. Sci., Part B: Polym. Phys.* **2004**, *42*, 1106.

NL061086I